Journal of Integrative Neuroscience

J. Integr. Neurosci. **2026**; 25(6): 47234
https://doi.org/10.31083/JIN47234

Original Research

Bone Marrow-Derived Mesenchymal Stromal Cells Alleviate Bone Cancer Pain by Modulating Microglial Polarization: Involvement of the Nrf2/HO-1 Pathway

Xinyu Lu[1,†], Penghui Ren[1,†], Jing Zhang[1], Ping Wu[1,*], Qingping Wen[1,*]

[1]Department of Anesthesiology, The First Affiliated Hospital of Dalian Medical University, 116000 Dalian, Liaoning, China
*Correspondence: 13684559453@163.com (Ping Wu); qingping_wen@yahoo.com (Qingping Wen)
[†]These authors contributed equally.

Academic Editor: Vincent Lelievre
Submitted: 10 October 2025 Revised: 2 April 2026 Accepted: 17 April 2026 Published: 28 June 2026

Abstract

Background: Dysregulated polarization of spinal microglia is a key contributor to the pathophysiology of bone cancer pain (BCP). Bone marrow-derived mesenchymal stromal cells (BMSCs) have demonstrated significant analgesic and microglial-modulatory effects in various pain models. The nuclear factor erythroid 2-related factor 2 (Nrf2)/heme oxygenase-1 (HO-1) signaling pathway is implicated in the regulation of microglial polarization. However, the specific role and mechanistic basis of intrathecally administered BMSCs in influencing spinal microglial polarization during BCP remain to be fully clarified. In this study, we investigated the impact of intrathecal administration of BMSCs on spinal microglial polarization in a rat model of BCP, and assessed the potential contribution of the Nrf2/HO-1 signaling pathway to this process. **Methods**: In a rat model of BCP, animals received three intrathecal injections of 2×10^6 BMSCs at every other day. Pain behavioral tests, including measurements of the 50% paw withdrawal threshold (PWT) and the number of spontaneous flinches (NSF), were assessed before and after BMSCs administration. The CatWalk automated gait analysis system was employed to quantify BMSC-mediated amelioration of BCP-associated locomotor deficits. Protein expression levels of the pro-inflammatory microglial markers cluster of differentiation 86 (CD86) and inducible nitric oxide synthase (iNOS), along with the anti-inflammatory markers CD206 and Arginase-1 (Arg-1), as well as key components of the Nrf2/HO-1 signaling pathway, were measured in spinal cord tissues using Western blot and immunofluorescence staining. In addition, a non-contact co-culture system of BMSCs and lipopolysaccharide (LPS)-activated BV2 cells was established. The expression of CD86, iNOS, CD206, Arg-1, and pathway components, together with the mRNA levels of the inflammatory cytokines interleukin (IL)-1β and IL-10, were analyzed via Western blot, immunofluorescence, and quantitative real-time PCR (RT-qPCR). **Results**: Intrathecal injection of BMSCs significantly alleviated established pain behaviors in BCP rats, as evidenced by increased 50% PWT, reduced NSF, and normalized gait parameters. At the molecular level, BMSC treatment downregulated the spinal cord expression of the pro-inflammatory markers CD86 and iNOS while concurrently upregulating the anti-inflammatory markers CD206 and Arg-1. In the co-culture system, BMSC enhanced the activation of the Nrf2/HO-1 signaling pathway within LPS-stimulated BV2 cells. This enhancement was associated with a reduction in the expression of CD86 and iNOS, an increase in CD206 and Arg-1, decreased levels of IL-1β, and elevated levels of IL-10. **Conclusions**: Intrathecal administration of BMSCs effectively attenuates pain in BCP rats by shifting spinal microglial polarization from a pro-inflammatory toward an anti-inflammatory phenotype. The observed modulation of microglial polarization by BMSCs is consistent with an involvement of the Nrf2/HO-1 signaling pathway.

Keywords: bone cancer pain; bone marrow-derived mesenchymal stromal cells; microglia; Nrf2/HO-1 pathway

1. Introduction

Bone cancer pain (BCP) is a severe and often intractable type of pain resulting from bone metastasis in patients with advanced breast, lung, or prostate cancer, significantly impairing their quality of life [1,2]. Current clinical management of BCP follows the World Health Organization (WHO) analgesic ladder, primarily relying on nonsteroidal anti-inflammatory drugs (NSAIDs) and opioids for pain control [3]. However, long-term use of these drugs can lead to systemic adverse effects such as nausea, vomiting, constipation, gastrointestinal ulcers, and hepatorenal toxicity, along with the risks of opioid tolerance and addiction [4,5]. These intolerable side effects often necessitate discontinuation of therapy, resulting in inadequate pain relief. Therefore, there exists a critical and unmet need to develop alternative, better-tolerated strategies for BCP management.

The mechanisms of BCP are complex. They include the compression, infiltration, and destruction of peripheral sensory nerve endings by tumor tissue and its locally acidic microenvironment. This process sensitizes peripheral nociceptive neurons and triggers neuroinflammatory responses and central sensitization at both the spinal and supraspinal levels [6]. Within the pathogenesis of BCP, neuroinflammatory processes occurring in the dorsal horn of the spinal cord occupy a position of central importance. The exces-

sive activation of spinal glial cells precipitates the release of a plethora of inflammatory mediators, which in turn drives the sensitization of pain-transmitting neurons [7]. Within the central nervous system, microglia function as resident, macrophage-like immune sentinels. They are primary mediators of the intrinsic immune response triggered by neural damage or pathological conditions [8]. Substantial evidence now positions aberrant microglial activation as a critical mechanistic component in BCP and a promising point for therapeutic intervention [9,10,11]. In the context of BCP, activated spinal microglia predominantly adopt a pro-inflammatory polarization state, accompanied by a relative diminution of anti-inflammatory activity and the excessive production of pro-inflammatory cytokines such as interleukin (IL)-1β and tumor necrosis factor-α (TNF-α) [12]. Thus, therapeutic strategies aimed at rebalancing excessive microglial activation and correcting this polarization imbalance hold significant potential for BCP treatment.

The transcription factor nuclear factor erythroid 2-related factor 2 (Nrf2) serves as a master regulator of cellular antioxidant responses and plays a pivotal role in controlling the expression of genes involved in anti-inflammatory processes [13]. A key downstream effector of Nrf2 is the enzyme heme oxygenase-1 (HO-1), which catalyzes the degradation of heme to generate carbon monoxide, biliverdin, and free iron. This reaction confers not only direct antioxidant and anti-apoptotic benefits but also contributes to the suppression of inflammatory signaling by inhibiting the activation of the NOD-like receptor pyrin domain containing 3 (NLRP3) inflammasome and the subsequent release of pro-inflammatory cytokines, thereby promoting immune homeostasis [14,15]. Preclinical research has established that pharmacological or genetic activation of the Nrf2/HO-1 pathway yields potent analgesic effects in various pain models [16,17]. Moreover, pathway activation can favorably modulate microglial polarization, driving a shift from a pro-inflammatory to an anti-inflammatory phenotype and ameliorating neuroinflammation [18]. Therefore, targeting the Nrf2/HO-1 signaling pathway emerges as a promising strategy to rectify the imbalance in microglial polarization that contributes to BCP.

Bone marrow-derived mesenchymal stromal cells (BMSCs) are multipotent stromal cells widely present in the bone marrow of mammals. Their potent anti-inflammatory and immunomodulatory properties have generated significant attention in the field of pain research [19,20,21].

Importantly, the mechanism by which BMSCs attenuate BCP involves the suppression of pathological microglial activation [22]. However, a detailed understanding of how intrathecally delivered BMSCs influence the specific polarization imbalance of microglia in the setting of BCP remains incomplete. To address this gap, the present study was undertaken to investigate the effects of intrathecal BMSCs administration on microglial polarization states within the spinal cord of BCP rats and in a complementary *in vitro* microglial activation system, with a parallel aim of assessing the involvement of the Nrf2/HO-1 signaling pathway in this regulatory process.

2. Materials and Methods

2.1 Animals

The study used female Sprague-Dawley rats with an initial body weight of 200 ± 20 g. These animals were supplied by Changsheng Bio-technology Co., Ltd. (Lianyungang, Jiangsu, China). Rats were acclimatized for a period of seven days within a specific pathogen-free (SPF) facility at the Experimentation Center of Dalian Medical University. Housing conditions were rigorously controlled and maintained at a temperature of 22 ± 2 °C, a relative humidity of 55 ± 5%, and under a 12-hour light/dark cycle. Standard rodent chow and filtered water were provided. 18 rats were randomly allocated into three experimental groups (n = 6 per group): (1) SHAM, (2) BCP, and (3) BMSCs group. By administering 3% isoflurane, euthanasia was performed. All procedures involving animals were conducted in strict accordance with the approved guidelines, the 3R principles, and the reporting standards outlined in the ARRIVE guidelines 2.0, with the objectives of minimizing animal usage and alleviating potential distress.

2.2 Preparation of Walker 256 Cells

The Walker 256 rat mammary carcinoma cell line served as the source for establishing the BCP model. This cell line was a generous gift from Professor Dong Changsheng of the Shanghai Institute of Traditional Chinese Medicine. Prior to use, the cells were validated by STR profiling and confirmed to be free of mycoplasma contamination through testing with a dedicated PCR-based detection kit (C0301S, Beyotime, Shanghai, China).

Cells were routinely cultured in a humidified incubator (set at 37 °C with 5% CO_2) in high-glucose DMEM medium (11965092, Gibco, Waltham, MA, USA) enriched with 10% fetal bovine serum (FSP500, Excell, Suzhou, China) and 1% penicillin-streptomycin (15140122, Gibco, Waltham, MA, USA). A suspension containing 5×10^6 Walker 256 cells (in 0.5 mL) was administered via intraperitoneal injection into rats (80–100 g). Ascites was harvested 5–7 days post-injection, followed by centrifugation at 300 ×g for 5 minutes and red blood cell lysis (R1010, Solarbio, Beijing, China). Finally, the pelleted cells were washed and resuspended in ice-cold PBS at 1×10^5 cells/μL for subsequent applications.

2.3 Establishment of the BCP Rat Model

Before initiating the model induction, all rats underwent screening for mechanical allodynia and spontaneous pain. Only animals exhibiting normal baseline pain thresholds were included in the subsequent procedures. The BCP model was established following an established protocol [23]. In brief, anesthesia was induced with 3% isoflurane

(R510-22, RWD, Shenzhen, Guangdong, China), and the left hind limb surgical site was prepared with 75% ethanol. The patellar ligament was exposed through a 0.5–1 cm knee joint incision. The tibial bone marrow cavity was accessed by inserting a 23-gauge needle through the tibial plateau. This needle was then carefully exchanged for a 10 µL Hamilton microsyringe to administer 5 µL of the freshly prepared Walker 256 cell suspension (1×10^5 cells/µL). Hemostasis and closure were achieved by sealing the puncture site with sterile bone wax and closing the skin incision using sterile sutures. SHAM group rats underwent an identical procedure but received a 5 µL intra-tibial injection of sterile PBS instead of cells.

2.4 Preparation and Characterization of BMSCs

Rat BMSCs utilized in this study were sourced from the Stem Cell Bank of the Chinese Academy of Sciences (Catalog No. SCSP-402). Prior to experimental use, the absence of mycoplasma contamination in the cell stock was verified using a commercial PCR-based detection kit (C0301S, Beyotime, Shanghai, China). Third-passage cells were then cultured in MEM medium (C12571500BT, Gibco, Waltham, MA, USA) enriched with 10% fetal bovine serum (FSP500, Excell, Suzhou, Jiangsu, China) and 1% penicillin-streptomycin (15140122, Gibco, Waltham, MA, USA) at 37 °C with 5% CO_2. For surface marker analysis, BMSCs were incubated for 30 minutes at 4 °C with a panel of fluorescent antibodies: fluorescein isothiocyanate (FITC)-anti-cluster of differentiation (CD)29, phycoerythrin (PE)-anti-CD44, allophycocyanin (APC)-anti-CD90, PerCP-eF710-anti-CD11b/c (2702188, 12044181, 2311266, 46011082, eBioscience, San Diego, CA, USA), and Pacific Blue-anti-CD45 (202225, BioLegend, San Diego, CA, USA). Analysis was conducted using a flow cytometer (BD FACSAria III, BD Life Sciences, Milpitas, CA, USA). For analysis, negative populations were defined using unstained control cells from the same passage. The gating strategy was established to ensure that over 99.5% of events from the unstained control fell within the negative gate for each channel. To assess multilineage differentiation potential, BMSCs were treated with commercial induction kits for osteogenesis (hMODM-100, XRbiotech, Hangzhou, Zhejiang, China), adipogenesis, and chondrogenesis (H1016, H1017, Jinyuan, Shanghai, China) following the manufacturers' protocols. Post-induction, Alizarin Red S, Oil Red O, and Alcian Blue staining (ALIR-10001, OILR-10001, ALCB-10001, OriCell, Shanghai, China) were performed to detect osteogenic, adipogenic, and chondrogenic differentiation.

2.5 Intrathecal Injection of BMSCs

BMSCs (2×10^6 cells in 20 µL suspension) were delivered via intrathecal injection once daily on days 7, 9, and 11 after BCP model induction. Under anesthesia induced by 3% isoflurane, rats were positioned prone on a surgical platform. Following shaving and disinfection of the dorsal area with 75% ethanol, a 50 µL Hamilton microsyringe was carefully advanced through the intrathecal space between the L4 and L5 vertebrae. Correct placement was confirmed by a transient loss of resistance upon piercing the dura mater and, in some cases, by the aspiration of a small amount of clear cerebrospinal fluid. Following confirmation of proper needle placement, the BMSCs suspension was slowly infused. SHAM group animals underwent the identical procedure but received 20 µL of sterile PBS instead of cells.

2.6 X-ray Examination

Radiographic examination was performed on day 7 following intra-tibial inoculation of Walker 256 cells. Under 3% isoflurane anesthesia, rats were positioned in a prone posture with the left hind limb outstretched laterally. Bone destruction in the left tibia was assessed by scanning and imaging using the MultiFocus system (MultiFocus 2, Faxitron Bioptics LLC, Tucson, AZ, USA).

2.7 Hematoxylin-Eosin (HE) Staining

The left tibiae were collected on day 7 following intra-tibial inoculation of Walker 256 cells. The bone samples were fixed by immersion in 4% paraformaldehyde (BL539A, Biosharp, Beijing, China) for a duration of 48 hours at 4 °C. Subsequently, the fixed bones were decalcified by immersion in a 10% EDTA solution (E1171, Solarbio, Beijing, China) with the solution refreshed every 2–3 days, for a total period of two weeks. The decalcified tibiae were then processed for paraffin embedding (39601006, Leica, Wetzlar, Germany). Sectioning was performed sagittally at 4 µm thickness on a rotary microtome (RM2235, Leica), and collected onto poly-L-lysine-coated glass slides. The staining procedure involved deparaffinization in xylene, rehydration through a graded ethanol series, and application of reagents from a commercial HE Staining Kit (C0105S, Beyotime, Shanghai, China), strictly according to standardized protocol. Finally, slides were mounted with neutral balsam, and observation was performed using a bright-field microscope (BX53, Olympus, Tokyo, Japan) for image acquisition.

2.8 Behavioral Tests

Assessments for mechanical allodynia and spontaneous pain were conducted one day before the induction of the BCP model, with subsequent evaluations performed on post-inoculation days 4, 7, 9, 11, and 13. Testing occurred between 9:00 AM and 2:00 PM. The assessor was unaware of group allocations throughout the experiment. Prior to testing, a two-day habituation period to the environment was provided.

Mechanical allodynia testing utilized von Frey filaments (58011, Stoelting, Wood Dale, IL, USA), with the 50% paw withdrawal threshold (PWT) determined using the well-established Dixon up-down paradigm [24]. In

brief, each rat was individually placed in a transparent acrylic chamber positioned atop an elevated wire mesh grid and allowed to acclimate for 30 minutes. A blinded experimenter then applied a series of eight von Frey filaments, with bending forces ranging from 1.0 to 15.0 grams (specifically: 1.0, 1.4, 2.0, 4.0, 6.0, 8.0, 10.0, and 15.0 g), perpendicularly to the mid-plantar surface of the left hind paw. Each filament was applied until slight bending occurred and was held for 5–6 seconds, with a minimum inter-stimulus interval of 5 minutes. A sharp withdrawal or flinching of the paw during application was recorded as a positive response. The testing sequence followed the up-down paradigm: following the first change in response, an additional five stimuli were administered, with the filament force decreased one level after a positive response and increased one level after a negative response. The 50% PWT (in grams) was calculated offline using the formula: $50\%\ \mathrm{PWT} = 10^{(Xf+\kappa\delta)}$, where Xf represents the log value of the final filament used, κ is a tabulated value based on the pattern of responses, and δ is the mean logarithmic interval between filaments (0.224). If no response was elicited by the 15.0 g filament, a cutoff value of 15.0 g was assigned.

Spontaneous pain was evaluated by counting the number of spontaneous flinches (NSF) over a 2-minute period [25]. Each rat was placed alone in a transparent observation chamber. Any brisk lifting, shaking, or licking of the hind limb that was not associated with locomotion or grooming was counted as a spontaneous flinch. Each rat underwent five trials, with a rest interval of at least 10 minutes between consecutive trials. The mean NSF score from these five trials was used for subsequent analysis.

2.9 CatWalk Gait Analysis

On post-modeling day 13, gait function was evaluated using the CatWalk system (version 10.6, Noldus, Wageningen, The Netherlands) in accordance with a previously described protocol [26]. Individual rats were introduced into the apparatus from the open end of an enclosed corridor and encouraged to traverse it freely under illumination from red light-emitting diodes. Locomotor activity was recorded by a camera positioned below the transparent walkway floor, and the collected data were processed with the system's proprietary analysis software (version 10.0, Noldus, Wageningen, The Netherlands). A trial was deemed acceptable for analysis if it contained a minimum of three consecutive, complete step cycles or one full, uninterrupted traversal of the corridor. The analysis focused on two parameters relevant to BCP: (1) Max Contact Area, which refers to the greatest surface area of the hind paw in contact with the platform during a stance phase, and (2) Max Contact Max Intensity, denoting the peak pressure value detected at the instant of maximal paw contact. For each parameter, results are presented as the value obtained from the left hind paw expressed as a percentage of the corresponding value from the contralateral (right) hind paw.

2.10 Co-Culture of BMSCs and BV2 Cells

The microglial BV2 cell line (TCM-C718, HyCyte, Suzhou, Jiangsu, China) was used in this study. This cell line is well-characterized and widely used in neuroscience research. The cells typically exhibit a semi-adherent, amoeboid morphology with extending processes, consistent with activated microglia. Phenotypically verified, BV2 cells express characteristic microglial markers such as CD11b. The cell line was confirmed to be mycoplasma-free via PCR testing (Mycoplasma PCR Detection Kit, C0301S, Beyotime, Shanghai, China). Cells were maintained in DMEM (11965092, Gibco, Waltham, MA, USA) containing 10% fetal bovine serum (FSP500, Excell, Suzhou, China) and 1% penicillin-streptomycin (15140122, Gibco, Waltham, MA, USA) within a humidified incubator at 37 °C with 5% CO_2.

The co-culture was performed using 6-well plate format Transwell inserts featuring permeable membranes with a pore size of 0.4 µm (3470, Corning, Corning, NY, USA). The experimental design comprised four groups: (1) Control (CON) group : BV2 cells only (1×10^6 cells/well in lower chamber); (2) lipopolysaccharide (LPS) group: BV2 cells (1×10^6 cells/well in lower chamber) stimulated with 1 µg/mL LPS; (3) BMSCs group: BV2 cells (1×10^6 cells/well in lower chamber) treated with 1 µg/mL LPS and co-cultured with BMSCs (1×10^4 cells/well in upper chamber); (4) ML385 group: BV2 cells (1×10^6 cells/well in lower chamber) treated concurrently with 1 µg/mL LPS and the Nrf2 inhibitor ML385 (20 µM), and co-cultured with BMSCs (1×10^4 cells/well in upper chamber).

2.11 Immunofluorescence Staining

On day 13 following BCP model induction, rats received a terminal anesthesia with 3% isoflurane. Systemic perfusion was then performed via the left cardiac ventricle, sequentially using normal saline followed by 4% paraformaldehyde until the liver appeared uniformly pale. The L4–L6 segments of the spinal cord were dissected, post-fixed by immersion in 4% paraformaldehyde for 24 hours at 4 °C, and cryoprotected through immersion in a graded sucrose series (10%, 20%, 30%). Subsequently, tissues were embedded in Optimal Cutting Temperature (OCT) compound (BL557A, Biosharp, Beijing, China) and stored at −80 °C until sectioning. Coronal sections of the spinal cord were cut at a thickness of 20 µm using a cryostat (CM1950, Leica, Wilmington, DE, USA) and transferred onto adhesive microscope slides (188105W, Citotest, Haimen, Jiangsu, China). For immunofluorescence staining of spinal cord sections, in brief, slides were blocking in 5% goat serum (C0265, Beyotime) for 1 hour at room temperature and then incubated overnight at 4 °C with the following primary antibodies: mouse anti-ionized calcium-binding adapter molecule 1 (IBA-1, A27316, Abclonal, 1:300, Wuhan, Hubei, China), rabbit anti-inducible nitric oxide synthase (iNOS, AF0199, Affinity, 1:200), and rab-

bit anti-CD206 (DF4149, Affinity, 1:200). For staining of BV2 cells, cells were first rinsed three times with PBS and then fixed with 4% paraformaldehyde for 10 minutes at room temperature, permeabilized with 0.3% Triton X-100 (T8200, Solarbio) in PBS for 8 minutes, and blocked using a commercial blocking buffer (P0102, Beyotime) for 1 hour. The cells were subsequently incubated overnight at 4 °C with rabbit anti-Nrf2 primary antibody (80593-1-RR, Proteintech, 1:500, Rosemont, IL, USA). The following day, both tissue sections and cells were incubated with Alexa Fluor 488-conjugated secondary antibody (AB0141, Abways, 1:500, Shanghai, China) for 1 hour at room temperature. Additionally, sections stained for IBA-1 were incubated with an Alexa Fluor 594-conjugated secondary antibody (AB0152, Abways, 1:500, Shanghai, China). Nuclei were visualized by counterstaining with a 4′,6-diamidino-2-phenylindole (DAPI) mounting medium (ab104139, Abcam, Cambridge, UK). Fluorescent imaging was conducted on a CellVoyage CQ1 analysis system (Yokogawa, Tokyo, Japan). Quantitative analysis of fluorescence signals was performed by an investigator blinded to the experimental conditions utilizing ImageJ software (version 1.54, NIH, Bethesda, MD, USA). Data presented are the mean values derived from three independent experimental replicates.

2.12 Western Blot

Protein samples were extracted from the L4–L6 spinal cord segments of rats (day 13 post-modeling) and from harvested BV2 cells using radio-immunoprecipitation assay (RIPA) lysis buffer (P0013B, Beyotime, Shanghai, China) supplemented with protease/phosphatase inhibitors (P1045, Beyotime). Protein concentrations were determined with a bicinchoninic acid (BCA) assay kit (ZJ101, Epizyme, Cambridge, MA, USA). Equal amounts of protein (30 µg per lane) were resolved by sodium dodecyl sulfate–polyacrylamide gel electrophoresis (SDS-PAGE) and subsequently transferred onto polyvinylidene fluoride (PVDF) membranes (IPVH00010, Millipore, Billerica, MA, USA). The membranes were blocked with 5% non-fat milk in tris-buffered saline with tween 20 (TBST) for 1.5 hours at room temperature, followed by incubation overnight at 4 °C with the following primary antibodies: rabbit anti-CD86 (DF6332, Affinity, 1:1000, Jiangsu, China), rabbit anti-iNOS (AF0199, Affinity, 1:1000, Jiangsu, China), rabbit anti-Arginase-1 (Arg-1, 93668, Cell Signaling Technology, 1:1000, Danvers, MA, USA), rabbit anti-CD206 (DF4149, Affinity, 1:1000, Jiangsu, China), rabbit anti-Nrf2 (80593-1-RR, Proteintech, 1:1000, Wuhan, China), rabbit anti-HO-1 (AF5393, Affinity, 1:1000, Jiangsu, China), and rabbit anti-β-actin (GB15003, Servicebio, 1:3000, Wuhan, China). After washing, membranes were incubated with horseradish peroxidase (HRP)-conjugated secondary antibody (AS014, Abclonal, 1:5000, Wuhan, Hubei, China) for 1 hour at room temperature. Protein bands were visualized using an enhanced chemiluminescence substrate (WBKLS0500, Millipore, Darmstadt, Germany) and imaged with a ChemiDoc XRS+ system (1708265, Bio-Rad, Shanghai, China). Band intensities were quantified with ImageJ software (version 1.54, NIH) and normalized to β-actin. Data are presented as mean relative expression from three independent experiments. Uncropped Western blot images are provided in the **Supplementary Material**.

2.13 Quantitative Real-Time PCR (RT-qPCR)

Total RNA was isolated from BV2 cells using the SteadyPure Quick RNA Extraction Kit (AG21023, Accurate Biology, Changsha, Hunan, China) following provided protocol. Contaminating genomic DNA was eliminated, and first-strand cDNA was synthesized using the Evo M-MLV RT Mix Kit (AG11728, Accurate Biology, Hunan, China). RT-qPCR was performed on a 7500 Fast Real-Time PCR System (4351106, Thermo Fisher, Waltham, MA, USA) using the SYBR Green qPCR Kit II (AG11702, Accurate Biology). The CFX Manager software (version 3.0, Bio-Rad, Shanghai, China) was used for data acquisition and initial processing. To determine relative gene expression, the transcript levels of *IL-10* and *IL-1β* were normalized to glyceraldehyde-3-phosphate dehydrogenase (*GAPDH*). The comparative threshold cycle ($2^{-\Delta\Delta CT}$) method was used for relative quantification of target gene mRNA levels. The sequences for all gene-specific primers are provided in Table 1.

2.14 Statistical Analysis

All statistical analyses were conducted with GraphPad Prism software (version 10, GraphPad Software, Inc., San Diego, CA, USA). Quantitative data are expressed as the mean ± standard deviation (SD) derived from biologically independent replicates. The normality of data distribution and the homogeneity of variances were first verified using the Shapiro-Wilk test and Brown-Forsythe test, respectively. For the analysis of behavioral test outcomes, a two-way analysis of variance (ANOVA) was employed, with Tukey's test applied for post hoc comparisons involving three or more groups. Data obtained from CatWalk gait analysis, Western blot, and immunofluorescence experiments were assessed by one-way ANOVA, followed by either Tukey's or Dunnett's post hoc test for specific between-group comparisons. A two-tailed p value of less than 0.05 was considered statistically significant, denoted as $^{*}p < 0.05$, $^{**}p < 0.01$, and $^{***}p < 0.001$.

3. Results

3.1 BMSCs Characterization

Flow cytometric characterization revealed that BMSCs exhibited high positivity (>99%) for the markers CD29, CD44, and CD90. In contrast, expression levels of the hematopoietic lineage markers CD11b/c and CD45 were essentially undetectable (<1%) (Fig. 1A). Multilineage differentiation assays revealed that BMSCs formed mineral-

Table 1. Primer sequences used for quantitative real-time PCR (RT-qPCR).

Gene Symbol	Gene Name	Forward Primer (5′–3′)	Reverse Primer (5′–3′)
IL-10	Interleukin-10	GTAGAAGTGATGCCCCAGGC	GACACCTTGGTCTTGGAGCTTATT
IL-1β	Interleukin-1 beta	TTTGAAGTTGACGGACCCCAA	CACAGCTTCTCCACAGCCACA
GAPDH	Glyceraldehyde-3-phosphate dehydrogenase	CTGGAGAAACCTGCCAAGTATG	GGTGGAAGAATGGGAGTTGCT

ized nodules after 24 days of osteogenic induction, which stained red with Alizarin Red S. Following 16 days of adipogenic induction, BMSCs developed lipid vacuoles that appeared red with Oil Red O staining. After 28 days in chondrogenic induction medium, proteoglycan deposition was observed and stained blue with Alcian Blue (Fig. 1B–D). Collectively, these phenotypic and functional data verify that the BMSCs used in this study met the identification criteria for MSCs.

3.2 Successful Establishment of BCP Rat Model

The experimental design of this study is illustrated in Fig. 2A. The BCP rat model was established by intra-tibial inoculation of Walker 256 cells into the left tibia. Successful model induction was validated by measuring the 50% PWT and NSF one day before and on days 4, 7, 9, 11, and 13 post-inoculation. Compared to the SHAM group, rats in the BCP group demonstrated a sustained and significant reduction in 50% PWT alongside a concomitant increase in NSF from day 7 to day 13 post-inoculation (Fig. 2B,C). Furthermore, radiographic and histopathological assessments of the left tibiae were performed on day 7. Radiographic analysis showed that, in contrast to the continuous bone architecture and homogeneous density observed in SHAM rats, BCP rats showed clear signs of substantial osteolytic destruction, characterized by radiolucent lesions and defects primarily in the proximal tibia (Fig. 2D). Histological examination via HE staining corroborated these imaging findings. Tibial sections from SHAM controls exhibited normal, intact trabecular bone with normal cellular constituents within the marrow space. Conversely, tibiae from BCP rats displayed severe disruption of the trabecular network, evident osteolytic lacunae, and extensive infiltration of tumor cells within the marrow space (Fig. 2E). Taken together, these results confirmed that intra-tibial inoculation of Walker 256 cells reliably induced tibial bone destruction and sustained pain hypersensitivity from day 7 onward, thereby verifying the successful establishment of the BCP rat model.

3.3 Intrathecal Injection of BMSCs Alleviated Pain in BCP Rats

Both the present results and our preliminary data indicate that rats receiving intra-tibial inoculation of Walker 256 cells developed stable BCP by day 7 post-injection. Therefore, intrathecal administration of BMSCs was initiated on day 7 after model establishment. Based on our pre-experimental findings, which showed that a single intrathecal injection of 2×10^6 BMSCs provided analgesic effects lasting approximately two days in BCP rats, we administered BMSCs every other day for a total of three injections (on days 7, 9, and 11 post-tumor inoculation). Pain behaviors were assessed continuously throughout the treatment period. Measurements of 50% PWT and NSF were performed after each intrathecal injection and on day 2 after the final BMSCs injection. The results demonstrated that, compared to the BCP group, rats receiving intrathecal BMSCs exhibited a significantly increased 50% PWT and a markedly reduced NSF, with analgesic effects sustained through day 13 (Fig. 2B,C).

To assess pain-related functional deficits during voluntary movement, gait function was analyzed using the CatWalk system. Measurements of the maximal contact area and peak contact intensity for the hind paw were taken on the second day following the final BMSCs injection. A marked decrease in both parameters was observed in the BCP group relative to SHAM-operated controls. In contrast, rats receiving intrathecal BMSCs showed significant recovery in these gait metrics (Fig. 3A–D). It should be noted that this analysis was conducted with a sample size of n = 3 per group. While the observed differences were statistically significant, the relatively small sample size warrants caution in the interpretation of the effect size and suggests the need for validation in larger cohorts. These results demonstrate that intrathecal BMSC treatment effectively reversed gait disturbances associated with BCP. In summary, intrathecal administration of BMSCs effectively alleviated pain and improved functional outcomes in BCP rats.

3.4 Intrathecal Injection of BMSCs Attenuated Pro-inflammatory Polarization of Spinal Microglia in BCP Rats

To investigate the impact of intrathecal BMSCs on the polarization state of spinal microglia in BCP, we analyzed the expression of classical phenotypic markers at the protein level. Western blot analysis of spinal cord tissue harvested on day 2 after the final BMSCs injection revealed a distinct pattern. Compared to SHAM controls, the BCP model group exhibited a significant upregulation in the protein levels of both the pro-inflammatory markers CD86 and iNOS, as well as the anti-inflammatory markers Arg-1 and CD206. This broad upregulation suggests a state of generalized microglial activation in BCP. Notably, BMSCs treatment sig-

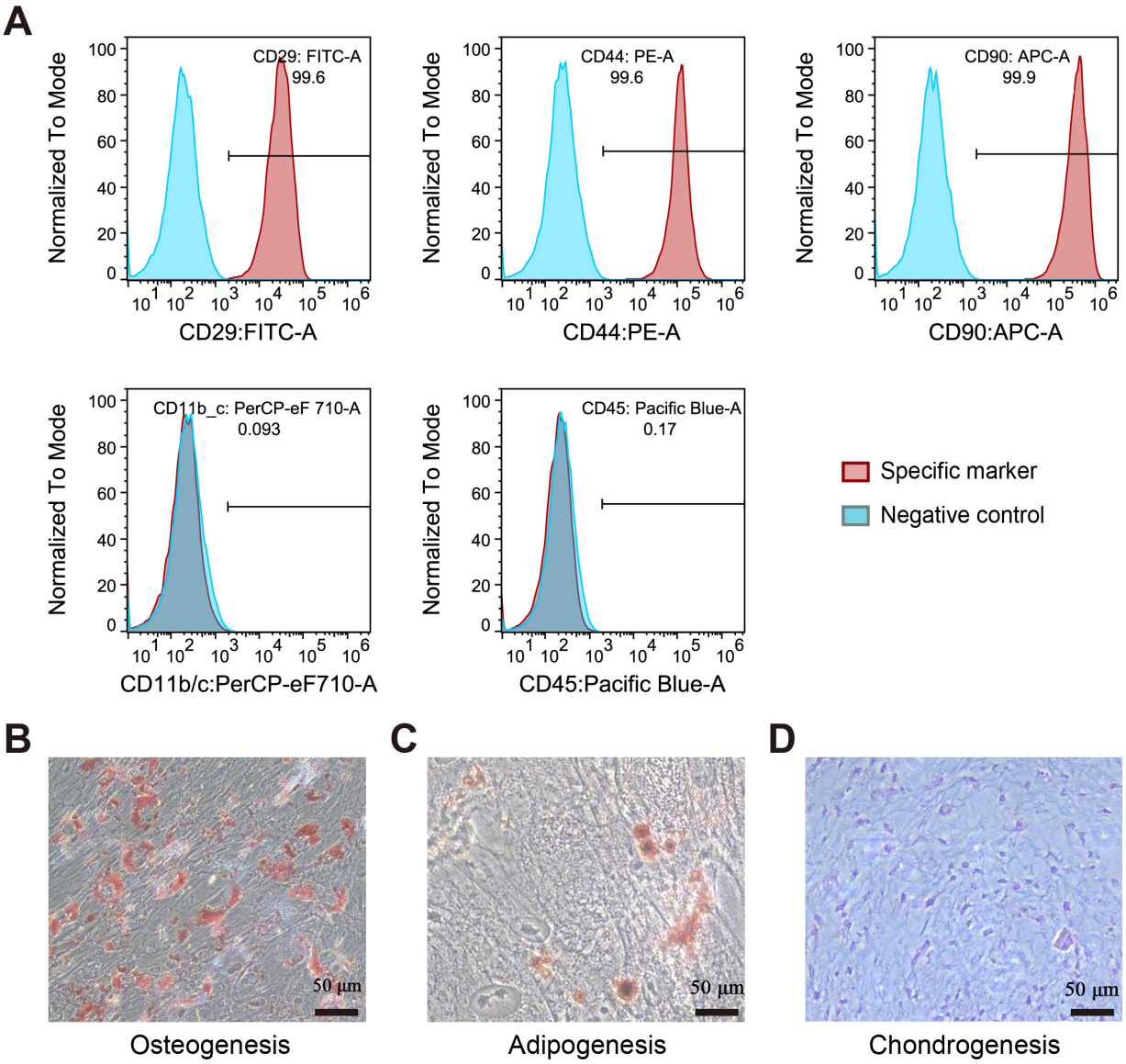

Fig. 1. Characterization of BMSCs. (A) Representative flow cytometry histograms of BMSCs markers. Data were normalized to the modal peak. (B) Osteogenic differentiation of BMSCs. (C) Adipogenic differentiation of BMSCs. (D) Chondrogenic differentiation of BMSCs. Scale bar: 50 μm. BMSCs, bone marrow-derived mesenchymal stromal cells; FITC, fluorescein isothiocyanate; PE, phycoerythrin; APC, allophycocyanin; CD, cluster of differentiation.

nificantly modulated this profile: it effectively suppressed the BCP-induced elevation of CD86 and iNOS, while simultaneously further augmenting the expression of Arg-1 and CD206 (Fig. 4A–F).

To corroborate these biochemical findings at the cellular level and to identify which specific microglial populations were affected, we performed immunofluorescence co-staining on spinal cord sections. Sections were double-labeled with antibodies against the pan-microglial marker IBA-1 and either the pro-inflammatory marker iNOS or the anti-inflammatory marker CD206. Quantitative analysis of the proportion of double-positive cells within the total IBA-1^+ microglial population provided clear cellular resolution. Consistent with the Western blot data, the BCP group showed a significant increase in the proportions of both $iNOS^+IBA\text{-}1^+$ and $CD206^+IBA\text{-}1^+$ microglia relative to the SHAM group. Critically, BMSC intervention exerted a divergent effect on these two subpopulations: it significantly reduced the percentage of $iNOS^+IBA\text{-}1^+$ microglia, while concurrently increasing the proportion of $CD206^+IBA\text{-}1^+$ microglia compared to the untreated BCP model (Fig. 4G–J). Together, these results indicated that intrathecal administration of BMSCs shifted the polarization state of spinal microglia in BCP rats, reducing the pro-inflammatory phenotype while enhancing the anti-inflammatory phenotype.

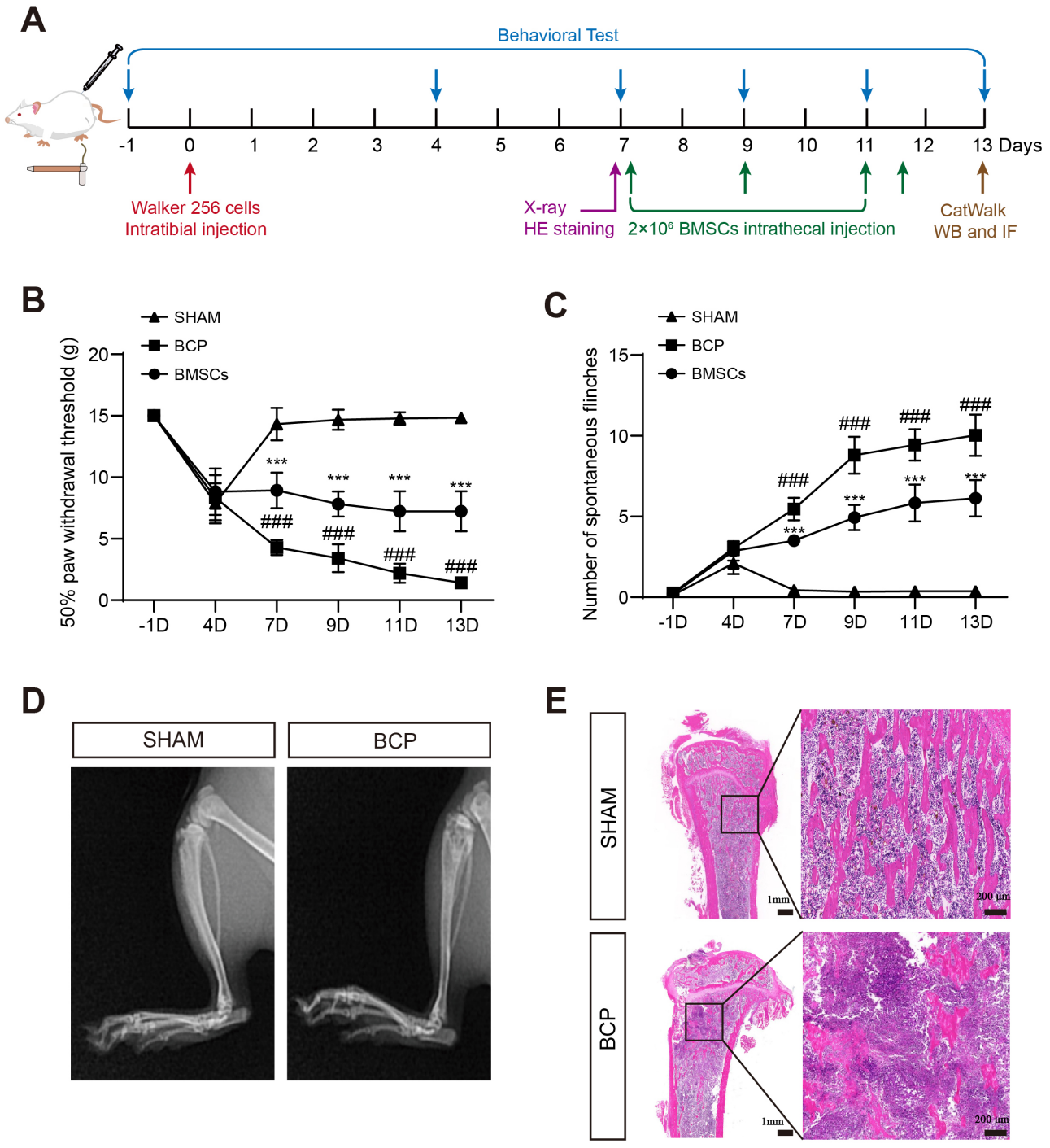

Fig. 2. Successful establishment of BCP rat model. (A) Experimental design. (B,C) 50% PWT and NSF at baseline (day -1) and on post-inoculation days 4, 7, 9, 11, and 13. (D) X-ray of left tibia on day 7 following intra-tibial inoculation. (E) Representative HE staining of left tibia on day 7 post-inoculation. Scale bars: 1 mm and 200 μm. $^{###}p < 0.001$ versus SHAM group, $^{***}p < 0.001$ versus BCP group ($n = 6$). BCP, bone cancer pain; HE, hematoxylin-eosin; WB, Western blot; IF, immunofluorescence.

3.5 Intrathecal Injection of BMSCs Activated the Nrf2/HO-1 Signaling Pathway in the Spinal Cord of BCP Rats

To determine whether intrathecal BMSCs administration modulates the spinal Nrf2/HO-1 signaling pathway of BCP rats, protein expression levels of Nrf2 and its downstream target HO-1 were evaluated by Western blot on day 2 after the final BMSCs injection. Analysis revealed that the expression of both Nrf2 and HO-1 proteins was markedly elevated in the BCP group relative to SHAM con-

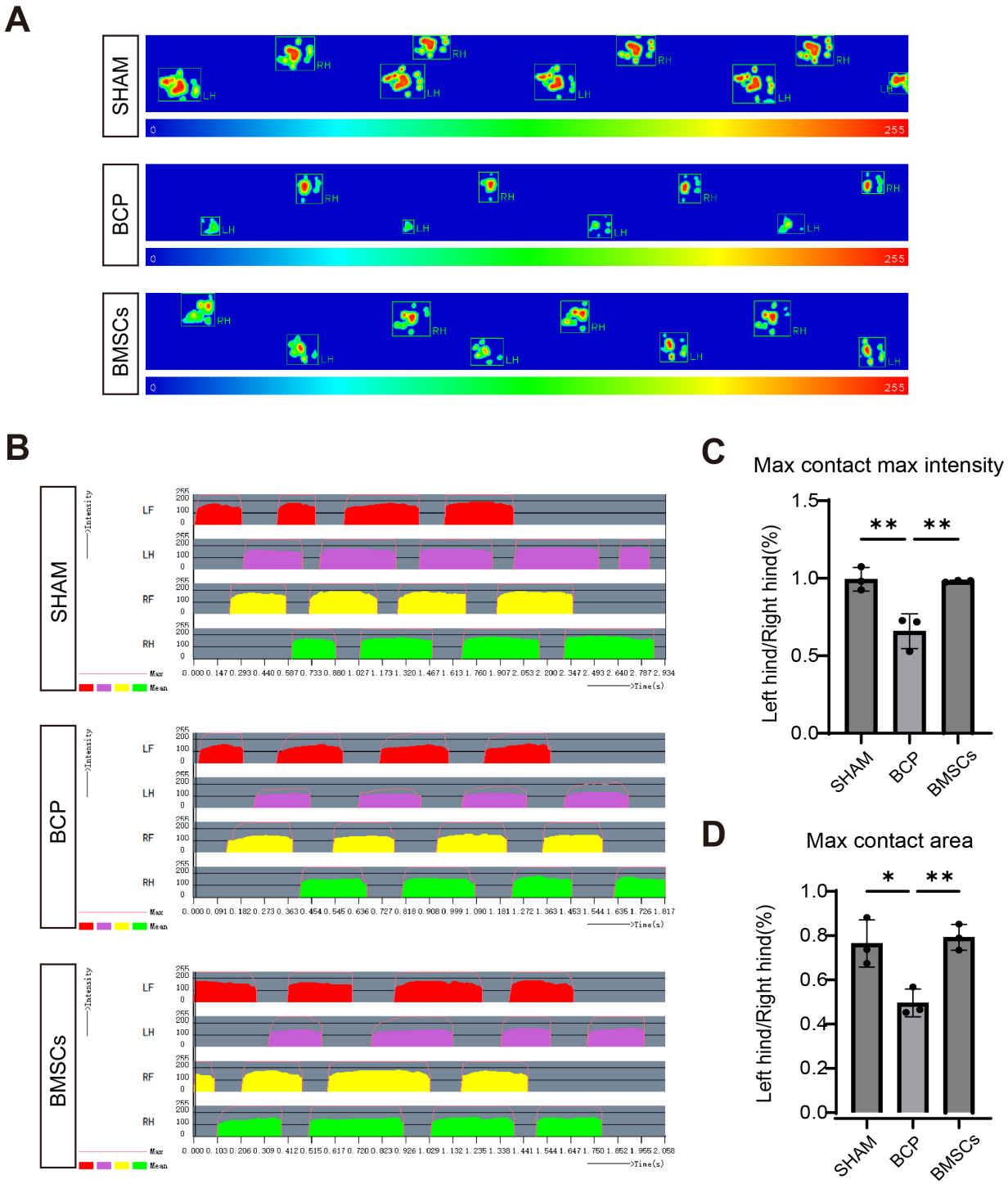

Fig. 3. Intrathecal injection of BMSCs alleviated pain in BCP rats. (A) Print view of CatWalk on day 2 after the final BMSCs injection. (B) Print intensity of CatWalk on day 2 after the final BMSCs injection. (C) Max contact max intensity for the left hind paw. (D) Max contact area for the left hind paw. Data are expressed as a percentage of the corresponding value from the right hind paw. *$p <$ 0.05, **$p < 0.01$ (n = 3). LF, left forepaw; LH, left hindpaw; RF, right forepaw; RH, right hindpaw.

trols. Moreover, this upregulation was further enhanced following intrathecal BMSCs treatment, resulting in significantly higher levels of both proteins compared to the BCP group alone (Fig. 5A–C). These data suggested that intrathecal BMSCs delivery activated the Nrf2/HO-1 signaling axis within the spinal cord under BCP conditions.

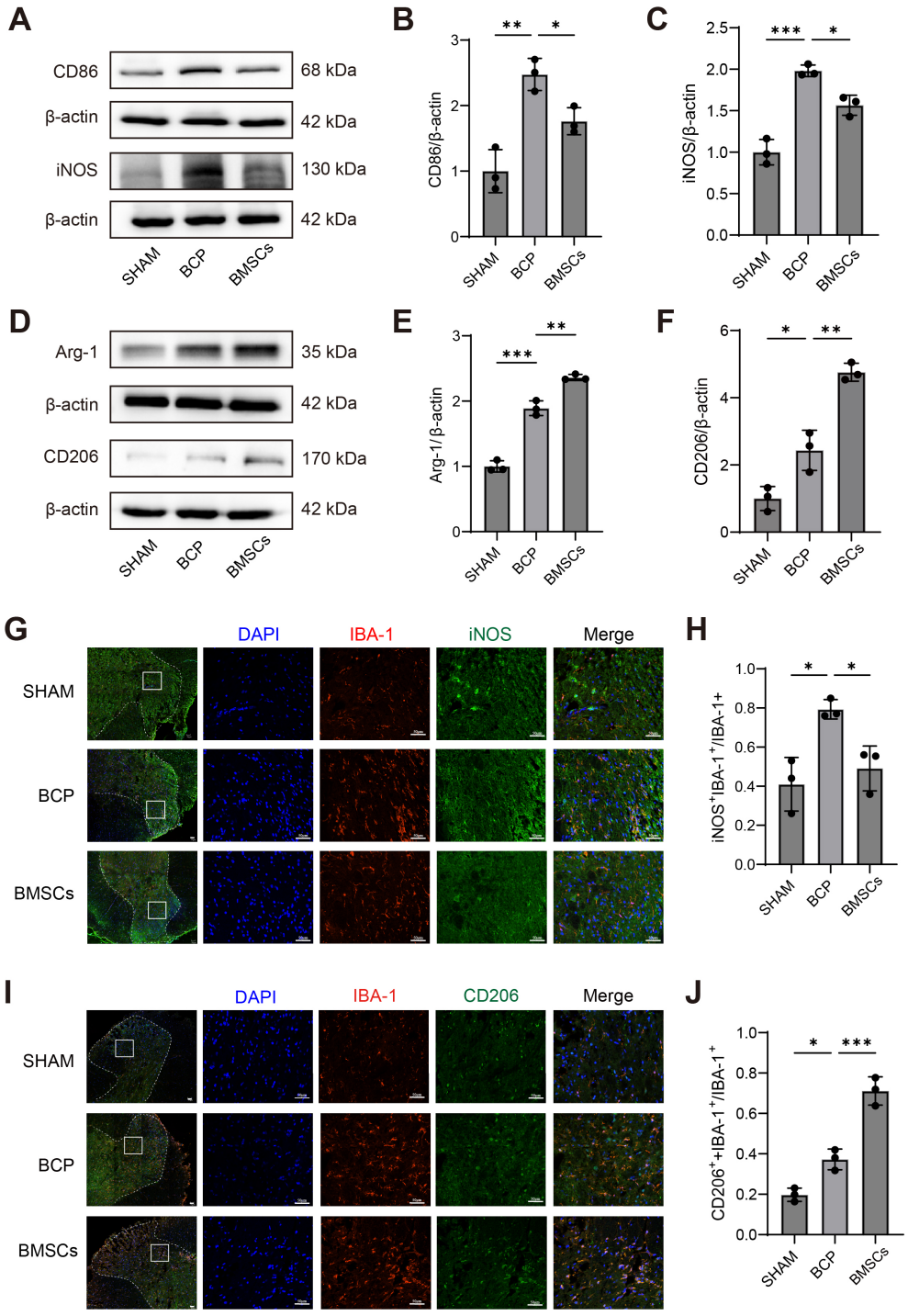

Fig. 4. Intrathecal injection of BMSCs attenuated pro-inflammatory polarization of spinal microglia in BCP rats. (A) Representative immunoblots of pro-inflammatory markers CD86 and iNOS protein levels in spinal cord on day 2 after the final BMSCs injection. (B) Relative CD86 protein level. (C) Relative iNOS protein level. (D) Representative immunoblots of anti-inflammatory markers Arg-1 and CD206 protein levels in spinal cord on day 2 after the final BMSCs injection. (E) Relative Arg-1 protein level. (F) Relative CD206 protein level. (G) Immunofluorescence co-staining of IBA-1 and iNOS in spinal cord on day 2 after the final BMSCs injection. (H) Quantitative analysis of $iNOS^+$ microglia. (I) Immunofluorescence co-staining of IBA-1 and CD206 in spinal cord on day 2 after the final BMSCs injection. (J) Quantitative analysis of $CD206^+$ microglia. Scale bar: 50 μm. $^*p < 0.05$, $^{**}p < 0.01$, $^{***}p < 0.001$ versus BCP group (n = 3). iNOS, inducible nitric oxide synthase; Arg-1, Arginase-1; IBA-1, ionized calcium-binding adapter molecule 1.

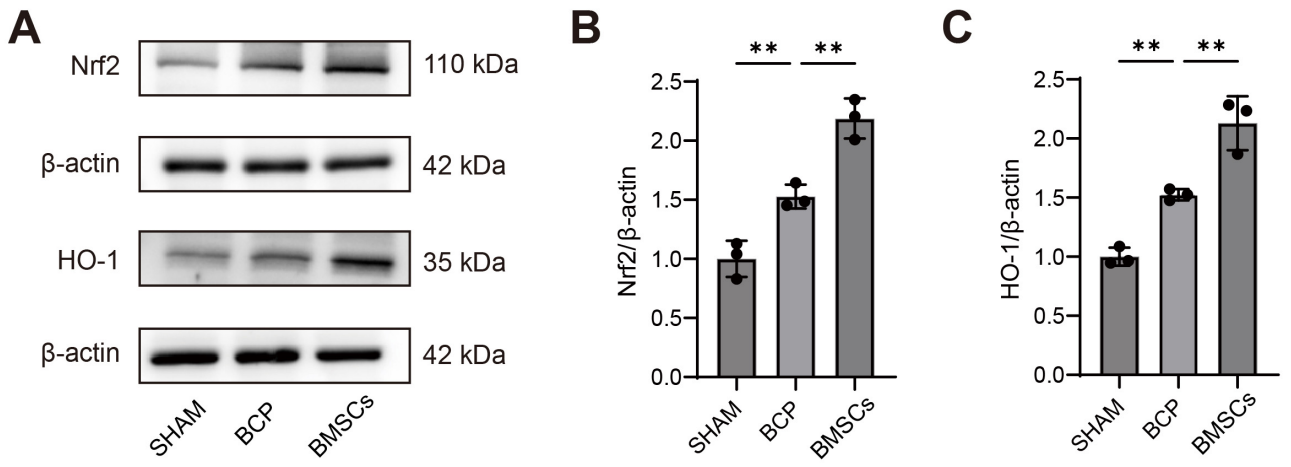

Fig. 5. Intrathecal injection of BMSCs activated the Nrf2/HO-1 signaling pathway in the spinal cord of BCP rats. (A) Representative immunoblots of Nrf2/HO-1 protein levels in spinal cord on day 2 after the final BMSCs injection. (B) Relative Nrf2 protein level. (C) Relative HO-1 protein level. $^{**}p < 0.01$ versus BCP group (n = 3). Nrf2, nuclear factor erythroid 2-related factor 2; HO-1, heme oxygenase-1.

3.6 BMSCs Activated the Nrf2/HO-1 Signaling Pathway in LPS-Stimulated BV2 Cells

To examine the capacity of BMSCs to regulate the Nrf2/HO-1 cascade in microglia, we implemented an indirect co-culture paradigm using a transwell system with BV2 cells (Fig. 6A). BV2 microglia were polarized toward an activated state via LPS stimulation. The impact of this co-culture on Nrf2 and HO-1 levels in BV2 cells was subsequently assessed by Western blot and immunofluorescence. Western blot indicated that LPS challenge notably upregulated the protein expression of both Nrf2 and HO-1 in BV2 cells relative to the untreated CON group. This upregulation was further potentiated when LPS-stimulated BV2 cells were co-cultured with BMSCs. Notably, the amplifying effect conferred by BMSCs co-culture was substantially suppressed by pre-treatment with the selective Nrf2 inhibitor, ML385 (Fig. 6B–D). Immunofluorescence analysis yielded congruent results, showing a significant increase in the mean fluorescence intensity of Nrf2 following LPS exposure compared to the CON group. Co-culture with BMSCs led to an additional enhancement of Nrf2 signal intensity over that induced by LPS alone, an effect that was similarly abolished in the presence of ML385. Examination of subcellular localization revealed a clear overlap of Nrf2 fluorescence with DAPI-stained nuclei, consistent with LPS-induced nuclear translocation of Nrf2, a process augmented by BMSCs co-culture (Fig. 6E,F). In summary, these findings substantiated that BMSCs promoted activation of the Nrf2/HO-1 pathway in LPS-stimulated BV2 cells.

3.7 BMSCs Attenuated Pro-Inflammatory Polarization of LPS-Stimulated BV2 Cells by Activating the Nrf2/HO-1 Signaling Pathway

To elucidate the mechanism by which BMSCs modulate microglial polarization, we focused on the Nrf2/HO-1 signaling axis. Protein expression of the polarization markers CD86, iNOS, Arg-1, and CD206 was evaluated by Western blot, while transcript levels of the cytokines IL-1β and IL-10 were measured by RT-qPCR in BV2 cells under various conditions. Western blot analysis indicated that exposure to LPS markedly upregulated the protein abundance of both pro-inflammatory (CD86, iNOS) and anti-inflammatory (Arg-1, CD206) markers in BV2 cells compared to the CON group. Notably, co-culture with BMSCs not only counteracted the LPS-induced elevation of CD86 and iNOS but also further augmented the expression of Arg-1 and CD206. The introduction of the specific Nrf2 inhibitor ML385 largely abolished these regulatory effects exerted by BMSCs (Fig. 7A–F). At the transcriptional level, RT-qPCR data showed that LPS stimulation significantly increased mRNA expression of both *IL-1β* and *IL-10* relative to the CON group. However, BMSC co-culture exerted a divergent effect: it significantly suppressed *IL-1β* mRNA levels while simultaneously promoting a further increase in *IL-10* expression compared to the LPS-only group. Again, pre-treatment with ML385 effectively reversed the modulatory influence of BMSCs on both cytokines (Fig. 7G,H). Collectively, findings indicated that BMSCs promoted a transition in microglial polarization from pro-inflammatory toward anti-inflammatory phenotype, an effect mediated through activation of the Nrf2/HO-1 pathway and reflected by the coordinated downregulation of IL-1β and upregulation of IL-10.

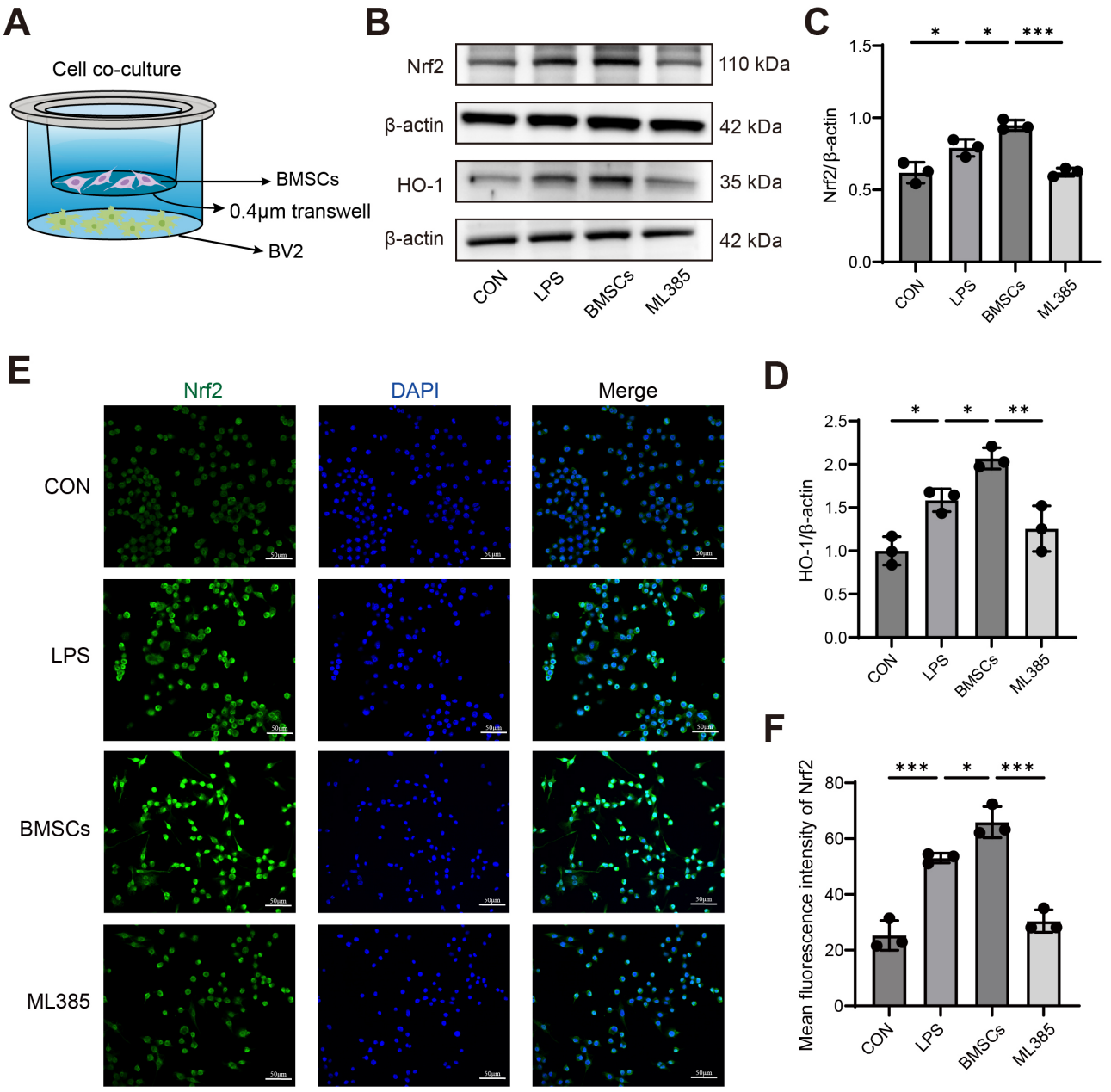

Fig. 6. BMSCs activated the Nrf2/HO-1 signaling pathway in LPS-stimulated BV2 cells. (A) Schematic diagram of the transwell system with BMSCs and BV2 cells. (B) Representative immunoblots of Nrf2/HO-1 protein levels in BV2 cells. (C) Relative Nrf2 protein level. (D) Relative HO-1 protein level. (E) Immunofluorescence staining of Nrf2 in BV2 cells. (F) Quantitative analysis of mean fluorescence intensity of Nrf2. Scale bar: 50 μm. *$p < 0.05$, **$p < 0.01$, ***$p < 0.001$ (n = 3). LPS, lipopolysaccharide; CON, control.

4. Discussion

This study was undertaken to explore the analgesic potential of intrathecal administration of BMSCs in BCP rats and their regulatory role in spinal microglial polarization. Our research indicates that intrathecal administration of BMSCs effectively alleviates pain in BCP rats. This therapeutic effect was associated with a modulation of microglial activation, characterized by a coordinated downregulation of markers associated with a pro-inflammatory phenotype and a concomitant upregulation of markers indicative of an anti-inflammatory phenotype. These effects are consistent with the involvement of the Nrf2/HO-1 pathway.

The intra-tibial inoculation of tumor cells is a well-established method for modeling BCP [23]. In the present study, we employed this approach by injecting Walker 256 mammary carcinoma cells directly into the tibial marrow cavity of rats. Previous reports have indicated that breast cancer cell-induced BCP is characterized by osteolytic bone destruction and progressive pain [27,28]. Our findings

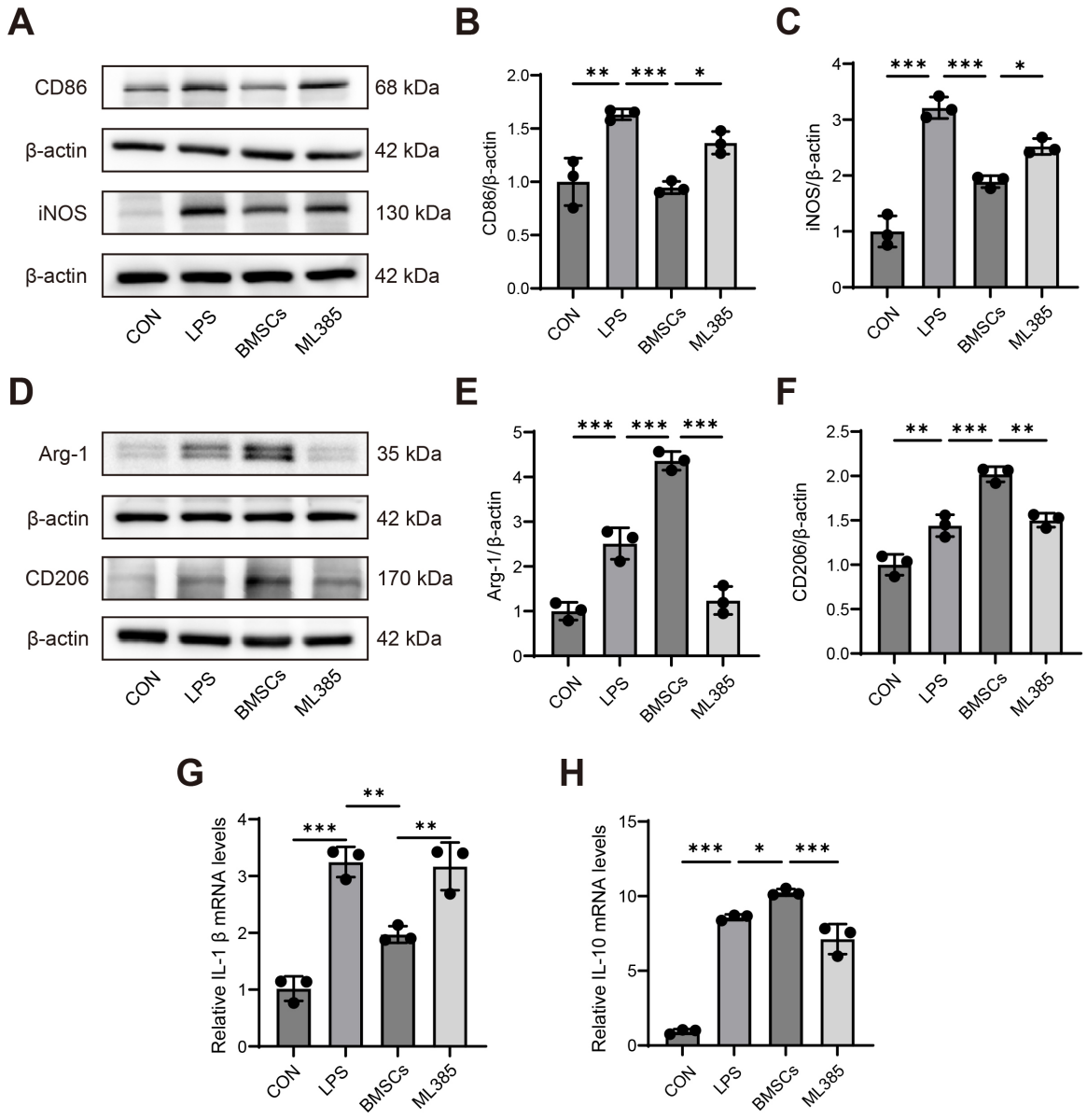

Fig. 7. BMSCs attenuated pro-inflammatory polarization of LPS-stimulated BV2 cells by activating the Nrf2/HO-1 signaling pathway. (A) Representative immunoblots of CD86 and iNOS protein levels in BV2 cells. (B) Relative CD86 protein level. (C) Relative iNOS protein level. (D) Representative immunoblots of Arg-1 and CD206 protein levels in BV2 cells. (E) Relative Arg-1 protein level. (F) Relative CD206 protein level. (G) Relative mRNA expression levels of *IL-1β*. (H) Relative mRNA expression levels of *IL-10*. *$p < 0.05$, **$p < 0.01$, ***$p < 0.001$ (n = 3).

aligned with these reports revealing a significant reduction in bone density and osteolytic defects in the trabecular bone seven days after tumor inoculation. Behavioral tests, including the 50% PWT and NSF, indicated sustained mechanical allodynia and spontaneous pain that did not resolve spontaneously. These observations are consistent with established features of BCP and confirm the successful establishment of the model.

Intrathecal BMSCs injections began on day 7 after intra-tibial inoculation, which was when stable pain hypersensitivity had developed. Our preliminary experiments showed that intrathecal administration of 2×10^6 BMSCs provided analgesic effects lasting about two days, indicating that multiple administrations may be necessary. Therefore, BMSCs were administered intrathecally on days 7, 9, and 11 post-inoculation. Behavioral assessments showed that this regimen effectively alleviated mechanical allodynia and spontaneous pain, with analgesia persisting for up to two days after the final injection. A study reported that intrathecal injection of 1×10^6 BMSCs relieved neuropathic

pain in mice for up to 31 days [29], whereas Kan et al. [22] observed pain relief lasting two days in a murine BCP model following the same dose. The comparatively shorter duration of analgesia in our BCP model, despite the higher dose and similar administration route, suggests that BCP may be more severe and refractory to treatment than neuropathic pain, potentially requiring higher or more frequent BMSC doses. Although differences between rodent species (rats vs. mice) may contribute to these disparities, our results indicate that the analgesic duration of 2×10^6 BMSCs in BCP may be limited by insufficient dosing.

CatWalk system provides an objective assessment of pain-induced gait abnormalities during voluntary locomotion. Multiple studies have validated the efficacy and reliability of this method for evaluating BCP in rat models. Quantifying parameters such as paw print area and pressure intensity during spontaneous walking allows accurate evaluation of analgesic interventions. Pain-affected animals typically exhibit reduced paw contact area and diminished pressure intensity [26,30]. Consistent with previous findings, our results demonstrated significant reductions in both max contact area and max contact intensity in BCP rats. Following intrathecal administration of BMSCs, these parameters were restored to near-normal levels. Thus, combined results from multiple behavioral tests confirm that intrathecal BMSCs injection effectively alleviates mechanical allodynia and spontaneous pain, while ameliorating gait abnormalities in BCP rats. These findings provide experimental evidence supporting BMSCs as a novel and promising therapeutic strategy for BCP.

As pivotal immune effector cells within the central nervous system, microglia and their phenotypic transitions during pain initiation and development have attracted considerable research interest [31,32]. Our previous study demonstrated that spinal microglia in BCP rats exhibit enhanced polarization toward a pro-inflammatory phenotype. This polarization imbalance contributes to inflammatory mediators and neuroinflammation at the spinal level, ultimately promoting central sensitization in BCP [33]. The present study focused on the dynamic changes in different polarization states of spinal microglia during BCP and investigated the effects of intrathecal BMSCs administration to rebalance the pro- and anti-inflammatory phenotypes. Although current understanding of microglial polarization has evolved beyond the simplistic M1/M2 dichotomy toward a continuum of heterogeneous states, the classical framework distinguishing pro- and anti-inflammatory phenotypes remains physiologically and pathologically relevant, providing valuable insights into their fundamental functions in pain modulation [34].

The pro-inflammatory phenotype is traditionally associated with elevated expression of markers such as CD86 and iNOS, along with the release of IL-1β, IL-6, and TNF-α, which promote hyperalgesia and allodynia [35,36]. In contrast, the anti-inflammatory phenotype expresses markers like CD206 and Arg-1 and secretes anti-inflammatory factors such as transforming growth factor β (TGF-β) and IL-10, contributing to immune suppression and tissue repair [37]. Notably, these two states are not mutually exclusive; they may dynamically coexist in a spatiotemporal manner and even exhibit transitional states and overlapping expression profiles, reflecting the plasticity of microglia within complex pathological microenvironments [38]. These concepts help interpret the findings of the present study. Our results demonstrated that in the spinal cord of BCP rats, microglia not only showed significantly elevated expression of pro-inflammatory phenotypic markers (CD86 and iNOS) but also exhibited concurrent upregulation of anti-inflammatory markers (CD206 and Arg-1). This phenomenon may arise from the following mechanisms. First, microglia may simultaneously initiate inflammatory responses and self-regulatory processes upon encountering early pain signals. Second, distinct microglial subpopulations might be concurrently activated, exhibiting either pro-inflammatory or anti-inflammatory functional biases, while tissue-level analyses detect an overall increase in multiple markers [38,39]. Thus, this seemingly paradoxical observation reflects the phenotypic diversity and dynamic complexity of microglial responses under BCP pathological conditions.

Our study further demonstrates that intrathecal administration of BMSCs significantly downregulated the expression of pro-inflammatory phenotypic markers while promoting the expression of anti-inflammatory markers in microglia. These findings suggest that BMSCs do not simply suppress overall microglial activation, but rather modulate their functional phenotype, potentially facilitating a transition from a destructive inflammatory response toward a reparative immune microenvironment. To explore the underlying mechanisms of this BMSC-mediated regulation, we focused on the Nrf2/HO-1 pathway in microglia. A previous study has established that the Nrf2/HO-1 pathway exerts potent anti-inflammatory and anti-nociceptive effects in various acute and chronic pain models induced by inflammation, nerve injury, or metabolic disorders [40]. Activation of this pathway has been shown to suppress microglial polarization toward a pro-inflammatory state [18]. In the present study, intrathecal BMSCs administration significantly increased the expression levels of both Nrf2 and its downstream effector HO-1 in the spinal cord of BCP rats. Combined with our observation that BMSCs promote anti-inflammatory microglial polarization, we hypothesize that BMSCs may facilitate a functional shift from pro- to anti-inflammatory states in microglia through activation of the Nrf2/HO-1 pathway, thereby contributing to their analgesic effects. Furthermore, it is noteworthy that our results revealed a significant upregulation of Nrf2 and HO-1 expression in the spinal cord of BCP rats even in the absence of BMSCs intervention. This phenomenon may be attributed to an endogenous compensatory mechanism initiated under

pathological conditions. The persistent inflammatory microenvironment in the spinal cord likely activates the Nrf2 anti-inflammatory response pathway, triggering a negative feedback loop to counteract excessive inflammation [41]. However, this compensatory upregulation appears insufficient to reverse the progression of BCP-related pain, suggesting that the endogenous response may be inadequate to fully restore immunological homeostasis without therapeutic augmentation.

To directly validate the necessity and specificity of the Nrf2/HO-1 pathway in mediating the BMSC-induced modulation of microglial polarization at the cellular level, we established a transwell co-culture system consisting of BMSCs and LPS-activated BV2 cells. Additionally, we used the Nrf2 inhibitor ML385 to suppress Nrf2/HO-1 pathway in the BV2 cells. LPS activation of BV2 cells is a well-established model for simulating polarized microglia in various neurological disorders and neuroinflammatory conditions, including pain and neural injury [36,42]. *In vitro* studies showed that LPS stimulation significantly increased the expression of Nrf2 and HO-1 in BV2 cells, leading to notable nuclear translocation of Nrf2. Under physiological conditions, Nrf2 is sequestered in the cytoplasm through binding to its repressor protein, Kelch-like ECH-associated protein 1 (Keap1). Inflammatory or oxidative stressors, such as those mimicked by LPS, promote the dissociation of Nrf2 from Keap1, allowing its translocation to the nucleus where it drives the transcription of cytoprotective genes including *HO-1* [41]. These findings align with our *in vivo* observations in BCP rats, further supporting the notion that microglia in BCP may activate an Nrf2-mediated endogenous stress response. Co-culture with BMSCs further enhanced the activation of the Nrf2/HO-1 pathway in LPS-stimulated BV2 cells, concurrently reducing their pro-inflammatory polarization (reducing CD86/iNOS) while promoting the anti-inflammatory polarization (increasing CD206/Arg-1). Specifically, BMSCs suppressed the release of the pro-inflammatory cytokine IL-1β and increased the production of the anti-inflammatory cytokine IL-10. All these effects were completely abolished by the Nrf2 inhibitor ML385. These results provide compelling evidence that BMSCs mitigate pro-inflammatory polarization of BV2 cells primarily through activation of the Nrf2/HO-1 signaling pathway.

This study has several limitations that should be addressed in future research. First, the cellular specificity of the Nrf2 pathway requires further validation. Our investigation primarily concentrated on verifying the role of the Nrf2/HO-1 pathway in the polarization of microglia mediated by BMSCs through *in vitro* studies. However, it is important to note that other spinal cell types, such as astrocytes and neurons, which also express Nrf2 *in vivo*, may play a significant role in regulating BCP. Future studies could employ microglia-specific conditional Nrf2 knockout mice to definitively establish the necessity and predominance of this pathway in microglial function and increase the sample size to confirm these functional outcomes. Second, the upstream and downstream mechanisms through which BMSCs activate the Nrf2/HO-1 pathway remain incompletely elucidated. Although our study confirmed that BMSCs promote Nrf2/HO-1 activation, the specific bioactive molecules involved, such as exosomes, cytokines, or chemokines, responsible for activating this pathway and modulating microglial polarization have yet to be identified. Future studies could delve deeper into the specific mediators. Furthermore, this study was conducted exclusively in female rats. The potential sexual dimorphism in the response to BMSCs therapy for BCP warrants future investigation in male subjects. The present study employed a single dose of BMSCs, future investigations exploring dose-response relationships and optimized delivery schedules are needed to maximize the durability of analgesic effects. Finally, our assessment of microglial polarization states relied on classical markers including CD86, iNOS, Arg-1, and CD206. Thus, our interpretation of microglial polarization in this study is based on these marker expression profiles, rather than on direct functional characterization of the cells. Future studies could integrate single-cell RNA sequencing technologies to resolve, at higher resolution, the heterogeneity of microglial subtypes and their dynamic transcriptional and functional transitions in response to BMSCs intervention. Such approaches would provide a more comprehensive theoretical foundation for developing targeted analgesic strategies directed against specific microglial subpopulations.

Safety considerations are crucial for translational potential. While our study demonstrates short-term efficacy, the translational application of intrathecal BMSC therapy requires careful safety assessment. Repeated intrathecal injections carry inherent risks such as infection and local inflammation. Furthermore, within the oncological context of BCP, the potential of MSCs to exert pro-tumorigenic effects through immune modulation or support of the tumor microenvironment warrants serious investigation. Future preclinical studies must include long-term monitoring for adverse events, dose-escalation safety profiles, and detailed evaluation of the fate of BMSCs and their potential tumor-modifying effects after intrathecal delivery.

5. Conclusions

This study demonstrates that intrathecal administration of BMSCs produces significant analgesia in BCP rats by shifting spinal microglial polarization balance from a predominantly pro-inflammatory state toward an anti-inflammatory phenotype. These effects are consistent with the involvement of the Nrf2/HO-1 pathway. Our findings not only elucidate a microglia-dependent mechanism for BMSC-induced analgesia but also highlight the Nrf2/HO-1 axis as a promising mechanistic target for developing novel treatments for BCP.

Availability of Data and Materials

The datasets used and analyzed in the present study are available upon request from the corresponding authors.

Author Contributions

XYL performed experiments and data analysis, wrote the main manuscript text, and prepared figures. PHR performed experiments and data analysis. JZ performed data analysis and prepared figures. PW designed the work, revised the manuscript, and contributed to funding acquisition. QPW designed the work, revised the manuscript, and contributed to funding acquisition. All authors contributed to editorial changes in the manuscript. All authors read and approved the final manuscript. All authors have participated sufficiently in the work and agreed to be accountable for all aspects of the work.

Ethics Approval and Consent to Participate

All animal experiments were approved by the Animal Ethics Committee of Dalian Medical University (Title of the approved project: Study on the Mechanism of Bone Marrow-Derived Mesenchymal Stromal Cells in Alleviating Bone Cancer Pain by Suppressing Microglial Activation and Neuroinflammation; Approval number: AEE24167; date of approval: 20 October 2024). The work has been reported in line with the National Institutes of Health Guide for the Care and Use of Laboratory Animals and the ARRIVE guidelines 2.0.

Acknowledgment

Not applicable.

Funding

This work was supported by the United Foundation for Dalian Institute of Chemical Physics, Chinese Academy of Sciences and the First Hospital of Dalian Medical University (DMU-1&DICP UN202402), the Liaoning Provincial Key Research and Development Program (2024JH2/102500038), and the Basic Scientific Research Project of Colleges and Universities of the Liaoning Provincial Department of Education (LJ212510161045).

Conflicts of Interest

The authors declare that they have no competing interests.

Supplementary Material

Supplementary material associated with this article can be found, in the online version, at https://doi.org/10.31083/JIN47234.

References

[1] Snijders RAH, Brom L, Theunissen M, van den Beuken-van Everdingen MHJ. Update on Prevalence of Pain in Patients with Cancer 2022: A Systematic Literature Review and Meta-Analysis. Cancers. 2023; 15: 591. https://doi.org/10.3390/cancers15030591

[2] Aielli F, Ponzetti M, Rucci N. Bone Metastasis Pain, from the Bench to the Bedside. International Journal of Molecular Sciences. 2019; 20: 280. https://doi.org/10.3390/ijms20020280

[3] Paice JA, Bohlke K, Barton D, Craig DS, El-Jawahri A, Hershman DL, et al. Use of Opioids for Adults With Pain From Cancer or Cancer Treatment: ASCO Guideline. Journal of Clinical Oncology : Official Journal of the American Society of Clinical Oncology. 2023; 41: 914–930. https://doi.org/10.1200/JCO.22.02198

[4] Bindu S, Mazumder S, Bandyopadhyay U. Non-steroidal anti-inflammatory drugs (NSAIDs) and organ damage: A current perspective. Biochemical Pharmacology. 2020; 180: 114147. https://doi.org/10.1016/j.bcp.2020.114147

[5] Colvin LA, Bull F, Hales TG. Perioperative opioid analgesia-when is enough too much? A review of opioid-induced tolerance and hyperalgesia. Lancet (London, England). 2019; 393: 1558–1568. https://doi.org/10.1016/S0140-6736(19)30430-1

[6] Zheng XQ, Wu YH, Huang JF, Wu AM. Neurophysiological mechanisms of cancer-induced bone pain. Journal of Advanced Research. 2021; 35: 117–127. https://doi.org/10.1016/j.jare.2021.06.006

[7] Falk S, Dickenson AH. Pain and nociception: mechanisms of cancer-induced bone pain. Journal of Clinical Oncology : Official Journal of the American Society of Clinical Oncology. 2014; 32: 1647–1654. https://doi.org/10.1200/JCO.2013.51.7219

[8] Salter MW, Stevens B. Microglia emerge as central players in brain disease. Nature Medicine. 2017; 23: 1018–1027. https://doi.org/10.1038/nm.4397

[9] Zhang WJ, Liu JP, Xu YS, Zuo C, Liao JX, Zhu FQ, et al. Olfactory ensheathing cell transplantation alleviates cancer pain by inhibiting P2X7 receptor expression-mediated activation of microglia. International Journal of Surgery (London, England). 2025; 111: 7727–7745. https://doi.org/10.1097/JS9.0000000000002976

[10] Huang LQ, Yan TX, Wang BS, Li H, Zhou NB. ZC3H15 suppression ameliorates bone cancer pain through inhibiting neuronal oxidative stress and microglial inflammation. Neoplasia (New York, N.Y.). 2025; 61: 101123. https://doi.org/10.1016/j.neo.2025.101123

[11] Apryani E, Ali U, Wang ZY, Wu HY, Mao XF, Ahmad KA, et al. The spinal microglial IL-10/β-endorphin pathway accounts for cinobufagin-induced mechanical antiallodynia in bone cancer pain following activation of α7-nicotinic acetylcholine receptors. Journal of Neuroinflammation. 2020; 17: 75. https://doi.org/10.1186/s12974-019-1616-z

[12] Dai J, Ding Z, Zhang J, Xu W, Guo Q, Zou W, et al. Minocycline Relieves Depressive-Like Behaviors in Rats With Bone Cancer Pain by Inhibiting Microglia Activation in Hippocampus. Anesthesia and Analgesia. 2019; 129: 1733–1741. https://doi.org/10.1213/ANE.0000000000004063

[13] Loboda A, Damulewicz M, Pyza E, Jozkowicz A, Dulak J. Role of Nrf2/HO-1 system in development, oxidative stress response and diseases: an evolutionarily conserved mechanism. Cellular and Molecular Life Sciences : CMLS. 2016; 73: 3221–3247. https://doi.org/10.1007/s00018-016-2223-0

[14] Bian H, Wang G, Huang J, Liang L, Zheng Y, Wei Y, et al. Dihydrolipoic acid protects against lipopolysaccharide-induced behavioral deficits and neuroinflammation via regulation of Nrf2/HO-1/NLRP3 signaling in rat. Journal of Neuroinflammation. 2020; 17: 166. https://doi.org/10.1186/s12974-020-01836-y

[15] Sun YY, Zhu HJ, Zhao RY, Zhou SY, Wang MQ, Yang Y, et al. Remote ischemic conditioning attenuates oxidative stress and

inflammation via the Nrf2/HO-1 pathway in MCAO mice. Redox Biology. 2023; 66: 102852. https://doi.org/10.1016/j.redox.2023.102852

[16] Petrikonis K, Bernatoniene J, Kopustinskiene DM, Casale R, Davinelli S, Saso L. The Antinociceptive Role of Nrf2 in Neuropathic Pain: From Mechanisms to Clinical Perspectives. Pharmaceutics. 2024; 16: 1068. https://doi.org/10.3390/pharmaceutics16081068

[17] Vasavda C, Xu R, Liew J, Kothari R, Dhindsa RS, Semenza ER, et al. Identification of the NRF2 transcriptional network as a therapeutic target for trigeminal neuropathic pain. Science Advances. 2022; 8: eabo5633. https://doi.org/10.1126/sciadv.abo5633

[18] Nan F, Tian Q, Chen S. Obacunone Alleviates Inflammatory Pain by Promoting M2 Microglial Polarization and by Activating Nrf2/HO-1 Signaling Pathway. Drug Design, Development and Therapy. 2024; 18: 1265–1275. https://doi.org/10.2147/DDDT.S451281

[19] Liu M, Yu W, Zhang F, Liu T, Li K, Lin M, et al. Fe3O4@Polydopamine-Labeled MSCs Targeting the Spinal Cord to Treat Neuropathic Pain Under the Guidance of a Magnetic Field. International Journal of Nanomedicine. 2021; 16: 3275–3292. https://doi.org/10.2147/IJN.S296398

[20] Schäfer S, Berger JV, Deumens R, Goursaud S, Hanisch UK, Hermans E. Influence of intrathecal delivery of bone marrow-derived mesenchymal stem cells on spinal inflammation and pain hypersensitivity in a rat model of peripheral nerve injury. Journal of Neuroinflammation. 2014; 11: 157. https://doi.org/10.1186/s12974-014-0157-8

[21] Zhu C, Wang K, Chen Z, Han Y, Chen H, Li Q, et al. Antinociceptive effect of intrathecal injection of miR-9-5p modified mouse bone marrow mesenchymal stem cells on a mouse model of bone cancer pain. Journal of Neuroinflammation. 2020; 17: 85. https://doi.org/10.1186/s12974-020-01765-w

[22] Kan H, Huang J, Gui X, Tian W, Fan L, Chen X, et al. Bone marrow mesenchymal stem cells improve bone cancer pain by inhibiting p38MAPK phosphorylation and microglia activation. The Korean Journal of Pain. 2025; 38: 116–127. https://doi.org/10.3344/kjp.24374

[23] Shen W, Hu XM, Liu YN, Han Y, Chen LP, Wang CC, et al. CXCL12 in astrocytes contributes to bone cancer pain through CXCR4-mediated neuronal sensitization and glial activation in rat spinal cord. Journal of Neuroinflammation. 2014; 11: 75. https://doi.org/10.1186/1742-2094-11-75

[24] Chaplan SR, Bach FW, Pogrel JW, Chung JM, Yaksh TL. Quantitative assessment of tactile allodynia in the rat paw. Journal of Neuroscience Methods. 1994; 53: 55–63. https://doi.org/10.1016/0165-0270(94)90144-9

[25] Ding Z, Liang X, Wang J, Song Z, Guo Q, Schäfer MKE, et al. Inhibition of spinal ferroptosis-like cell death alleviates hyperalgesia and spontaneous pain in a mouse model of bone cancer pain. Redox Biology. 2023; 62: 102700. https://doi.org/10.1016/j.redox.2023.102700

[26] Hu XM, Yang W, Du LX, Cui WQ, Mi WL, Mao-Ying QL, et al. Vascular Endothelial Growth Factor A Signaling Promotes Spinal Central Sensitization and Pain-related Behaviors in Female Rats with Bone Cancer. Anesthesiology. 2019; 131: 1125–1147. https://doi.org/10.1097/ALN.0000000000002916

[27] Song ZP, Xiong BR, Guan XH, Cao F, Manyande A, Zhou YQ, et al. Minocycline attenuates bone cancer pain in rats by inhibiting NF-κB in spinal astrocytes. Acta Pharmacologica Sinica. 2016; 37: 753–762. https://doi.org/10.1038/aps.2016.1

[28] Xu C, Wang Y, Ni C, Xu M, Yin C, He Q, et al. Histone modifications and Sp1 promote GPR160 expression in bone cancer pain within rodent models. EMBO Reports. 2024; 25: 5429–5455. https://doi.org/10.1038/s44319-024-00292-6

[29] Chen G, Park CK, Xie RG, Ji RR. Intrathecal bone marrow stromal cells inhibit neuropathic pain via TGF-β secretion. The Journal of Clinical Investigation. 2015; 125: 3226–3240. https://doi.org/10.1172/JCI80883

[30] Fuseya S, Yamamoto K, Minemura H, Yamaori S, Kawamata T, Kawamata M. Systemic QX-314 Reduces Bone Cancer Pain through Selective Inhibition of Transient Receptor Potential Vanilloid Subfamily 1-expressing Primary Afferents in Mice. Anesthesiology. 2016; 125: 204–218. https://doi.org/10.1097/ALN.0000000000001152

[31] Wu W, Zhang X, Wang S, Li T, Hao Q, Li S, et al. Pharmacological inhibition of the cGAS-STING signaling pathway suppresses microglial M1-polarization in the spinal cord and attenuates neuropathic pain. Neuropharmacology. 2022; 217: 109206. https://doi.org/10.1016/j.neuropharm.2022.109206

[32] Jin GL, Hong LM, Liu HP, Yue RC, Shen ZC, Yang J, et al. Koumine modulates spinal microglial M1 polarization and the inflammatory response through the Notch-RBP-Jκ signaling pathway, ameliorating diabetic neuropathic pain in rats. Phytomedicine : International Journal of Phytotherapy and Phytopharmacology. 2021; 90: 153640. https://doi.org/10.1016/j.phymed.2021.153640

[33] Wu P, Zhou G, Wu X, Lv R, Yao J, Wen Q. P2X7 receptor induces microglia polarization to the M1 phenotype in cancer-induced bone pain rat models. Molecular Pain. 2022; 18: 17448069211060962. https://doi.org/10.1177/17448069211060962

[34] Ochocka N, Kaminska B. Microglia Diversity in Healthy and Diseased Brain: Insights from Single-Cell Omics. International Journal of Molecular Sciences. 2021; 22: 3027. https://doi.org/10.3390/ijms22063027

[35] Gui X, Wang H, Wu L, Tian S, Wang X, Zheng H, et al. Botulinum toxin type A promotes microglial M2 polarization and suppresses chronic constriction injury-induced neuropathic pain through the P2X7 receptor. Cell & Bioscience. 2020; 10: 45. https://doi.org/10.1186/s13578-020-00405-3

[36] Zhao Y, Li T, Zhang L, Yang J, Zhao F, Wang Y, et al. TRAF6 promotes spinal microglial M1 polarization to aggravate neuropathic pain by activating the c-JUN/NF-kB signaling pathway. Cell Biology and Toxicology. 2024; 40: 54. https://doi.org/10.1007/s10565-024-09900-6

[37] Nakagawa Y, Chiba K. Diversity and plasticity of microglial cells in psychiatric and neurological disorders. Pharmacology & Therapeutics. 2015; 154: 21–35. https://doi.org/10.1016/j.pharmthera.2015.06.010

[38] Ransohoff RM. A polarizing question: do M1 and M2 microglia exist? Nature Neuroscience. 2016; 19: 987–991. https://doi.org/10.1038/nn.4338

[39] Cherry JD, Olschowka JA, O'Banion MK. Neuroinflammation and M2 microglia: the good, the bad, and the inflamed. Journal of Neuroinflammation. 2014; 11: 98. https://doi.org/10.1186/1742-2094-11-98

[40] Pol O. The role of carbon monoxide, heme oxygenase 1, and the Nrf2 transcription factor in the modulation of chronic pain and their interactions with opioids and cannabinoids. Medicinal Research Reviews. 2021; 41: 136–155. https://doi.org/10.1002/med.21726

[41] Tonelli C, Chio IIC, Tuveson DA. Transcriptional Regulation by Nrf2. Antioxidants & Redox Signaling. 2018; 29: 1727–1745. https://doi.org/10.1089/ars.2017.7342

[42] Sun S, Fan Z, Liu X, Wang L, Ge Z. Microglia TREM1-mediated neuroinflammation contributes to central sensitization via the NF-κB pathway in a chronic migraine model. The Journal of Headache and Pain. 2024; 25: 3. https://doi.org/10.1186/s10194-023-01707-w